



Endothelial delivery of antioxidant enzymes loaded into non-polymeric magnetic nanoparticles

Michael Chorny^{a,*}, Elizabeth Hood^{b,c,1}, Robert J. Levy^a, Vladimir R. Muzykantov^{b,c}

^a Department of Pediatrics, The Children's Hospital of Philadelphia, Abramson Research Bldg., Ste. 702, 3615 Civic Center Blvd., Philadelphia, PA 19104, USA

^b Institute for Translational Medicine and Therapeutics, University of Pennsylvania School of Medicine, 1 John Morgan Bldg/6068, 3620 Hamilton Walk, Philadelphia, PA 19104, USA

^c Institute for Environmental Medicine, University of Pennsylvania School of Medicine, 1 John Morgan Bldg/6068, 3620 Hamilton Walk, Philadelphia, PA 19104, USA

ARTICLE INFO

Article history:

Received 9 February 2010

Accepted 2 May 2010

Available online 18 May 2010

Keywords:

Antioxidant therapy

Antioxidant enzymes

Catalase

Superoxide dismutase

SOD

Nanocarrier

Nanoparticle

Drug Carriers

Nanotechnology

Magnetic delivery

Magnetic targeting

Superparamagnetic

Oxidative stress

Hydrogen peroxide

Endothelial cells

Controlled aggregation

Precipitation

ABSTRACT

Antioxidant enzymes have shown promise as a therapy for pathological conditions involving increased production of reactive oxygen species (ROS). However the efficiency of their use for combating oxidative stress is dependent on the ability to achieve therapeutically adequate levels of active enzymes at the site of ROS-mediated injury. Thus, the implementation of antioxidant enzyme therapy requires a strategy enabling both guided delivery to the target site and effective protection of the protein in its active form. To address these requirements we developed magnetically responsive nanoparticles (MNP) formed by precipitation of calcium oleate in the presence of magnetite-based ferrofluid (controlled aggregation/precipitation) as a carrier for magnetically guided delivery of therapeutic proteins. We hypothesized that antioxidant enzymes, catalase and superoxide dismutase (SOD), can be protected from proteolytic inactivation by encapsulation in MNP. We also hypothesized that catalase-loaded MNP applied with a high-gradient magnetic field can rescue endothelial cells from hydrogen peroxide toxicity in culture. To test these hypotheses, a family of enzyme-loaded MNP formulations were prepared and characterized with respect to their magnetic properties, enzyme entrapment yields and protection capacity. SOD- and catalase-loaded MNP were formed with average sizes ranging from 300 to 400 nm, and a protein loading efficiency of 20–33%. MNP were strongly magnetically responsive (magnetic moment at saturation of 14.3 emu/g) in the absence of magnetic remanence, and exhibited a protracted release of their cargo protein in plasma. Catalase stably associated with MNP was protected from proteolysis and retained 20% of its initial enzymatic activity after 24 h of exposure to pronase. Under magnetic guidance catalase-loaded MNP were rapidly taken up by cultured endothelial cells providing increased resistance to oxidative stress ($62 \pm 12\%$ cells rescued from hydrogen peroxide induced cell death vs. $10 \pm 4\%$ under non-magnetic conditions). We conclude that non-polymeric MNP formed using the controlled aggregation/precipitation strategy are a promising carrier for targeted antioxidant enzyme therapy, and in combination with magnetic guidance can be applied to protect endothelial cells from oxidative stress mediated damage. This protective effect of magnetically targeted MNP impregnated with antioxidant enzymes can be highly relevant for the treatment of cardiovascular disease and should be further investigated in animal models.

© 2010 Elsevier B.V. All rights reserved.

1. Introduction

Magnetically guided delivery strategies have the potential to enhance the therapeutic profile of a broad range of pharmaceuticals by increasing their distribution to the site of action, while minimizing off-target interactions [1]. Therefore, encapsulation in Magnetically-targeted NanoParticles (MNP) can increase efficiency and limit adverse effects of drug cargoes, facilitating the introduction of novel pharma-

cological interventions in clinical use. In support of this concept, the feasibility of using MNP for targeted delivery of small molecule pharmaceuticals, gene vectors, and cells has been addressed in a number of recent *in vitro* and animal model studies [2–6]. However, the utility and therapeutic potential of MNP for site-specific delivery of biologically active enzymes has remained largely unexplored due to considerable challenges in the design of such formulations.

Maintaining protein integrity and functionality in the process of nano- or microparticles formulation is not a trivial concern [7]. Stability of proteins incorporated in particulate systems based on biodegradable polymers, polylactide or poly(lactide-co-glycolide), has been investigated in a number of recent studies [8–10] using lysozyme, growth hormone, tetanus toxoid and growth factors as model cargoes. The primary mechanisms responsible for the compromised protein stability

* Corresponding author. The Division of Cardiology, The Abramson Pediatric Research Center, Suite 702G, The Children's Hospital of Philadelphia, 3615 Civic Center Blvd., Philadelphia, PA 19104, USA. Tel.: +1 215 590 3063; fax: +1 215 590 5454.

E-mail address: chorny@email.chop.edu (M. Chorny).

¹ Contributed equally to this work.

in these formulations have been shown to be related to the particle interior acidification due to autocatalytic degradation of the matrix polymer, as well as irreversible protein aggregation [7], both adversely affecting the structural integrity and biological activity of the encapsulated agents.

In this study a novel formulation method based on the use of a biocompatible fatty acid calcium salt as a non-polymeric particle matrix component was developed and applied to create a family of MNP further characterized *in vitro* as a platform for magnetically guided delivery of therapeutic enzymes. To combat the challenges of enzyme delivery, an ideal MNP formulation approach would not only enable loading of therapeutically adequate amounts of protein without compromising the biological activity, but would also create a sub-micron sized, magnetically responsive, biocompatible carrier structure that provides protection from potential proteolytic deactivation while allowing permeability for the enzyme substrate.

To design such MNP we chose antioxidant enzymes, catalase and superoxide dismutase (SOD), as model biotherapeutics. These enzymes consist of several subunits (two in SOD, Mw 36 kD, and four in catalase, Mw 240 kD) and contain active centers with coordinated metals, which decompose superoxide anion and hydrogen peroxide, respectively, i.e., reactive oxygen species (ROS) that are postulated to cause vascular oxidative stress involved in pathogenesis of many maladies, including hypertension, stroke, ischemia, inflammation, myocardial infarction and restenosis [11–14]. ROS are small molecules that have been shown to diffuse almost as rapidly across synthetic materials that are used to form nanocarriers as they do across biological membranes [15]. Therefore, encapsulated enzymes retain the capacity to decompose their substrates while remaining protected from proteolytic degradation.

Enzyme-loaded non-polymeric MNP were formulated in the present study by the controlled aggregation/precipitation method using mild aqueous conditions, and the key features of this new protein delivery platform were investigated, including the magnetic properties, enzymatic activity and capacity to protect cargo proteins from proteolysis. Additionally, we tested the hypothesis that under magnetic guidance MNP can efficiently deliver catalase to cultured vascular endothelial cells, and thereby provide therapeutically adequate protection against oxidative stress.

2. Materials and methods

2.1. Reagents

Ferric chloride hexahydrate, ferrous chloride tetrahydrate, sodium oleate (99% pure), Pluronic F-127, xanthine, xanthine oxidase, 2-(N-morpholino) ethane sulfate (MES), and pronase were purchased from Sigma-Aldrich (St Louis, MO). Uranyl acetate was from Electron Microscopy Sciences. Catalase and Cu, Zn superoxide dismutase, both from bovine liver, were purchased from Calbiochem (La Jolla, CA). Iodogen and Dylight 488 NHS ester were purchased from Pierce Biotechnology (Rockford, IL). Other reagents were purchased from Fisher Scientific (Pittsburgh, PA).

2.2. Enzyme preparation and iodination

Solid bovine liver catalase was dissolved in deionized water (Direct-Q 5 System, Millipore, Billerica, MA) and dialyzed in sodium free phosphate buffer using a slide-a-lyzer dialysis cassette (Thermo Scientific, Rockford IL). SOD was dissolved in PBS to desired concentrations. Final protein concentrations were determined spectrophotometrically ($\lambda = 595$ nm; Cary 50 UV-vis, Varian, Palo Alto, CA) against calibration curves obtained with bovine serum albumin (BSA) using a standard Bradford assay as described previously [16].

Catalase and SOD were radiolabeled with Na- 125 I (Perkin Elmer, Boston, MA) using the Iodogen method as described by the

manufacturer (Pierce Biotech., Rockford, IL), and purified from unbound iodine using gel permeation chromatography (Biospin 6 Columns, Bio-Rad Labs, Hercules, CA). The procedure was modified for labeling SOD that has only two tyrosine residues in its sequence susceptible for radiolabeling at pH 7.4. By using Tris buffer at pH 8.4 we were able to also tag histidine residues (pK_A 6.5) and increase the radiolabeling efficiency. The extent of labeling and amount of free iodine were determined for both proteins using a standard trichloroacetic acid (TCA) assay. A 2 μ l aliquot of labeled enzyme, 1.0 ml BSA (3%) and 0.2 ml TCA (100%) were vortexed and incubated at RT for 15 min. Precipitated protein was separated from free iodine supernatant by centrifugation (15 min, 4 °C, 2100 g) and measured using a Wizard 1470 gamma counter (Wallac Oy, Turku, Finland).

Fluorescent labeling of catalase with Dylight 488 was carried out as described by the manufacturer using the amine reactive N-hydroxysuccinimide (NHS) derivative of the dye.

2.3. MNP formulation and characterization

Nanocrystalline mixed iron oxide (magnetite) was prepared by coprecipitation of ferrous and ferric chlorides (62.5 and 170 mg, respectively) from ethanol solution (2.5 ml) with an equivalent amount of aqueous sodium hydroxide (0.5 N, 5.0 ml). Iron oxide was matured by incubation for 1 min at 90 °C, then washed twice with deionized water by magnetic decantation on ice, and finally resuspended in 5 ml of an aqueous solution containing 225 mg of sodium oleate with 2 cycles of heating to 90 °C under argon and bath sonication (5 min each). The obtained ferrofluid was filtered through sterile membranes with a 5 μ m and 0.45 μ m cut-off connected in a tandem mode. All subsequent formulation steps were carried out in sterile conditions using 0.2 μ m-filtered reagent solutions.

To prepare enzyme-loaded MNP, protein was added to the ferrofluid at a specified amount. A controlled aggregation of the ferrofluid was carried out in the presence of Pluronic F-127 (20 mg) as a stabilizer by dropwise addition of an equal volume of aqueous calcium oleate (0.1 M). MNP were washed twice by magnetic decantation and finally resuspended in 0.75 ml of aqueous glucose solution (5% w/v). Radioactive-labeled formulations were prepared by admixing a fraction of 125 I labeled catalase to the protein prior to the controlled aggregation step. Enzyme-impregnated non-magnetic nanoparticles or blank MNP used as controls were prepared as described above without incorporation of iron oxide or enzyme, respectively. Non-magnetic particles were purified using microcentrifuge 0.22 μ m filter units (Millipore, Billerica MA) and washed 3 times with a 5% glucose solution in calcium and magnesium free PBS.

2.3.1. Particle size, zeta potential, concentration and magnetic behavior

Particle zeta potential and size were measured using 90Plus Particle Sizer and Zeta Potential Analyzer (Brookhaven Instruments, Holtsville, NY). Zeta potential was determined at different pH conditions following MNP dilution 1:1000 in either Tris or MES buffer (pH 7.5 and 5.5, respectively). Particle size distributions and mean hydrodynamic radii of nanoparticles diluted $\times 200$ –400, were derived from the second order diffusion coefficient obtained from the Stokes–Einstein equation. This measure is independent of particle morphology and refractive index and is derived directly from the scattering intensity data. Particle number concentration was calculated by mass balance using experimentally determined density of the sample solution, dry weight, and size of the particles.

For transmission electron microscopy (TEM; JEOL JEM-100CX TEM West Chester, PA), 2–5 μ l of MNP sample diluted 20-fold in 0.2 μ m filtered deionized water was added to individual TEM mesh grids (Formvar Film 200 mesh, Electron Microscopy Sciences, Hatfield, PA), excess sample was wiped with filter paper. Grids were dried in a vacuum desiccator for at least 1 h before they were imaged with an accelerating voltage of 80 keV.

To determine the magnetic behavior of MNP, 5 μ l of the suspension were air-dried on a cover glass slide, and hysteresis measurements were made using an alternating gradient magnetometer (Princeton Measurements Corp., NJ).

2.3.2. Iron concentration

The amount of magnetite incorporated in the particles was measured in triplicate samples against a calibration curve constructed from a 1:2 molar mixture of ferrous and ferric chlorides in a range of 0.1–25.0 mg/ml. Ten- μ l samples were added to 1.0 ml hydrochloric acid (6 M) and 10 μ l hydrogen peroxide (3 wt.%) and allowed to react in the dark for 1 h. Light absorption was read at 410 nm.

2.3.3. Enzyme loading

The incorporation of protein in MNP was determined by measuring the distribution of the radiolabeled SOD or catalase between magnetically separated MNP and the external aqueous phase using a gamma counter. Percentage retained is defined as the quotient of the activity in the final sample to that of the original suspension adjusted for volume changes.

2.3.4. Enzyme activity

Catalase activity was determined using a standard hydrogen peroxide degradation assay. PBS-buffered 5 mM hydrogen peroxide solution (990–998 μ l) was added to a quartz cuvette and the absorbance was read at $\lambda = 242$ nm at room temperature. Catalase containing particles were diluted to a final catalase concentration of ~ 0.01 – 0.50 μ g/ml corresponding to the linear region of the calibration plot where the slope of the decay curve was proportional to the concentration of the catalase added. Two to ten μ l of MNP were typically diluted to make a total volume of 1.0 ml. The concentration of the hydrogen peroxide was monitored over time and the activity of the catalase was calculated from the slope of the decay curve where 1 activity unit = 23 (Δ Abs/t) [17].

SOD activity was determined using the ferricytochrome *c* assay as previously described [18,19]. The cytochrome *c* assay uses xanthine and xanthine oxidase to generate superoxide anion with cytochrome *c* acting as an indicating scavenger which competes with SOD. A reaction solution was prepared using 50 mM phosphate buffer, pH 7.8, 0.1 μ M EDTA, 50 μ M xanthine, 20 μ M cytochrome *c* and 10 μ l sample. The reaction was initiated by the addition of 10 μ l of 0.2 U/ml xanthine oxidase. The absorbance was monitored at 550 nm. One unit of SOD is defined as the amount of enzyme that inhibits the rate of cytochrome *c* reduction by 50% at pH 7.8 and 25 °C.

2.3.5. Protection and activity of MNP-encapsulated catalase

The capacity of MNP to protect catalase cargo was measured using a proteolysis assay. Samples were incubated for 60 min at 37 °C with shaking in a 0.2 wt.% buffered Pronase, a robust mixture of proteases with wide range of substrate specificities. The amount of catalase retained by MNP post proteolysis was determined following MNP separation by centrifugation (20 min, 4 °C at 16.1 g) using the radioactivity assay described above. The enzymatic activity of MNP-bound catalase retained over time was measured as described in Section 2.3.4 in comparison with free catalase.

2.3.6. Catalase in vitro release from MNP

The release kinetics of catalase from MNP was measured at physiological temperature by monitoring free catalase in the release medium using the radioactivity assay. Equal volumes of particle suspensions and mouse plasma were combined and placed in a 37 °C shaker bath. Aliquots were taken over a 48 hour period and MNP were separated from the medium using 0.2 μ m centrifugal filter units (Millipore, Billerica MA.). A correction was made for the fraction of MNP determined in the filtrate (<10%). The radioactivity of MNP-bound catalase retained by the filters and free protein in the medium were measured using a gamma counter.

2.4. Cell culture

Bovine aortic endothelial cells (BAEC) were obtained as previously described [20] and cultured in DMEM (Mediatech, Inc., Herndon, VA, USA) supplemented with 10% fetal calf serum. Primary human umbilical vein endothelial cells (HUVEC, Clonectics, San Diego, CA), 4th passage, grown to near confluence were cultured on 1% gelatin-coated 24 well plates. Cells were maintained in M199 media (Gibco, Grand Island, NY) supplemented with 15% fetal bovine serum and 100 μ g/ml heparin (Sigma), 0.1% endothelial cell growth supplement (Upstate, Lake Placid, NY), 0.1 μ g/ml Glutamax, and 1.0% antibiotic–antimycotic (Gibco).

2.4.1. Magnetically guided delivery of MNP to BAEC

BAEC seeded at confluence on a 96-well plate were incubated with blank or catalase-loaded MNP (0–5 μ g/well) for 10 min with/without the presence of a high gradient magnetic field using a 96-well magnetic separator with an average cross-sectional force density of 5.6 T²/m as a magnetic field source (LifeSepTM 96F, Dexter Magnetic Technologies, Fremont, CA, USA). The cells were then washed twice, incubated with fresh cell culture medium and examined microscopically for MNP internalization 4 h post treatment. The uptake of MNP-bound catalase was visualized by fluorescent microscopy using MNP formulated with Dylight 488-labeled catalase (FITC channel).

To determine the amount of internalized MNP, iron oxide was assayed spectrophotometrically ($\lambda = 370$ nm) following cell lysis with hydrochloric acid (37% w/v) against a calibration curve obtained by spiking MNP with untreated BAEC for background correction. Cell viability was determined 24 h post treatment using the Cell-Titer Blue assay (Promega, Madison, WI) vs. untreated cells used as a reference. To measure their growth kinetics, cells treated with MNP under magnetic conditions as above were trypsinized and seeded at 15% of confluency on a 96-well plate. The cell number was measured in triplicates using a hemocytometer on days 1, 4, 7 and 10 in comparison with untreated cells.

2.4.2. Magnetically enhanced protection of HUVEC from oxidative stress by MNP

Confluent HUVEC seeded on 24-well plates were incubated at 37 °C with 1 ml of catalase-loaded magnetic or non-magnetic nanoparticles diluted in cell culture media to a concentration equivalent to 10 μ g catalase/ml. Free catalase, blank MNP or their mixture applied at equivalent dosages were used as controls. The incubation was carried out with or without a magnetic exposure for 15 min. Following incubation cells were rinsed and treated for 5 h with 10 mM hydrogen peroxide diluted in cell culture medium, then washed with fresh medium, and stained for 15 min with a 2 μ M solution of a viability marker, Calcein AM (Invitrogen, CA), in PBS supplemented with Ca²⁺ and Mg²⁺. The fluorescence of viable cells was measured at $\lambda_{em} / \lambda_{ex}$ of 485 nm/535 nm.

2.5. Statistical analysis

Experimental data were analyzed using a two variable heteroscedastic student *t*-test. Cell protection results were evaluated for statistical significance by the Kruskal–Wallis one-way analysis of variance on ranks with Dunn's post hoc test. Differences were termed significant at $p < 0.05$.

3. Results

3.1. MNP size and magnetic properties

Catalase-loaded MNP were formed with an average size of 303 \pm 38 nm per digital analysis of multiple TEM images (example in Fig. 1A). In agreement with these results, dynamic light scattering

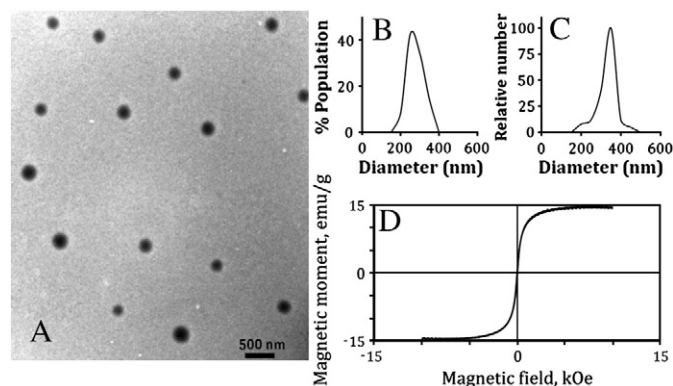


Fig. 1. Physicochemical properties of magnetic nanoparticles. A. TEM image of MNP. B. MNP size distribution measured by multiple TEM images analyzed with ImageJ software. C. MNP size distribution measured by dynamic light scattering. D. Hysteresis curve of MNP determined using alternating gradient magnetometer. The closed loop through the origin indicates perfect superparamagnetic behavior.

analysis of equivalent formulations showed that MNP had a mean hydrodynamic size of 340 ± 29 nm (Fig. 1B and C). The zeta potential of blank and catalase-loaded MNP revealed a similar dependence on pH, equaling -7.9 ± 1.3 mV and -9.3 ± 1.1 mV at pH 7.5, and $+8.6 \pm 0.8$ mV and $+9.7 \pm 0.6$ mV at pH 5.5, respectively.

The incorporation of magnetite at ~ 21 wt.% as measured by colorimetric assay endowed MNP with strong magnetic responsiveness (magnetic moment at saturation of 14.3 emu/g, Fig. 1D) in the absence of significant residual magnetization (magnetic remanence of 0.65 emu/g). The closed hysteresis loop (Fig. 1D) suggests a superparamagnetic behavior, with no magnetic moment retained by MNP upon removal of the magnetic field.

3.2. Protein loading by mass and enzymatic activity

SOD-loaded MNP exhibited a hydrodynamic diameter similar to that of catalase-impregnated MNP (350 ± 10 nm) with no statistical difference between the two formulations formed with SOD input of

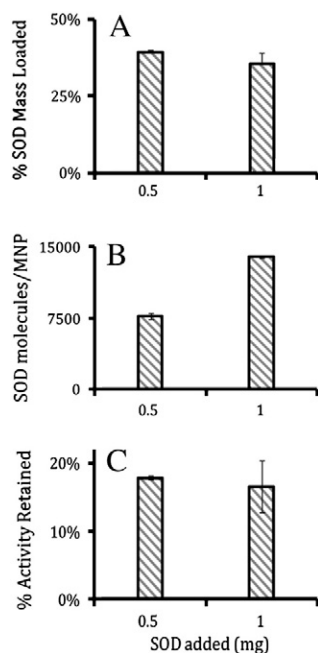


Fig. 2. MNP loaded with SOD. A. % SOD activity retained relative to mass added. B. % Mass of SOD loaded relative to mass SOD added. C. Calculated number of SOD molecules per particle based on SOD mass loading.

Table 1
Properties of catalase-loaded MNP.

Catalase added (mg)	Diameter (nm)	% Catalase loaded	% Catalase protected	% Catalase activity retained	Catalase molecules/MNP
0	336 ± 15				
0.2	341 ± 29	24.1 ± 9.8	29 ± 1.0	29.4 ± 1.0	310
2.0	365 ± 29	20.4 ± 0.6	11.4 ± 0.4	23.1 ± 0.6	2600
4.0	$399 \pm 14^*$	33.0 ± 5.0	22.7 ± 2.1	33.9 ± 4.8	8500
6.0	$385 \pm 3.0^{**}$	28.0 ± 3.0	25.9 ± 2.3	20.2 ± 4.2	7800

Error is standard deviation; $n \geq 3$. Size difference $^*p = 0.0145$, $^{**}p = 0.0017$ compared to blank MNP.

0.5 and 1.0 mg ($p = 0.39$). The loading efficiency of SOD in MNP expressed as a fraction of initially added protein that remains associated with MNP following the purification steps was $39 \pm 1\%$, $34 \pm 1\%$ for 0.5 and 1.0 mg SOD amounts, respectively (Fig. 2A, $p = 0.09$, $n = 3$). This fractional loading corresponds to an average of 7500 and 15,000 SOD molecules per individual MNP in the respective formulations as calculated from the protein mass loaded (Fig. 2B). MNP-encapsulated SOD exhibited enzymatic activity equivalent to $17 \pm 2\%$ of that of initially used protein suggesting that SOD loaded in MNP retains approximately 50% of its enzymatic activity (Fig. 2C).

The properties of catalase-loaded MNP as a function of the protein formulation input were characterized in a separate set of experiments (See Table 1). With a fractional loading efficiency ranging from 20 to 33%, protein amount loaded in MNP showed a near linear dependence on the catalase input (Fig. 3A). Within the studied protein input range this corresponds to an estimated number of 300 to 8500 catalase molecules associated with individual particles (Table 1). Catalase loading by mass and activity in non-magnetic nanoparticles was found to be similarly efficient to that in MNP.

The enzymatic activity of MNP-encapsulated catalase determined as a function of the protein input exhibited a saturation pattern reaching its maximum of about 12 ± 2 kUnits (Fig. 3B), which indicates that catalase loaded in MNP retains approximately 35% of its enzymatic activity (Table 1).

3.3. Release kinetics and protection of MNP-encapsulated catalase from proteolytic degradation

The initial release of catalase from MNP in plasma occurred *in vitro* at a higher rate compared to that in isotonic aqueous solution of

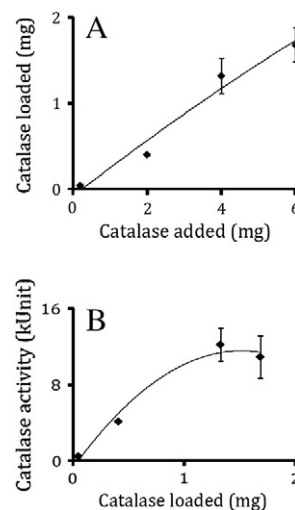


Fig. 3. Catalase loading and catalytic activity as a function of the enzyme mass addition. A. Catalase loading versus input measured by radiotracing of ^{125}I -catalase shows a near-linear relationship. B. Activity of loaded catalase as measured by degradation of hydrogen peroxide absorbance at 242 nm over time reaches saturation at ~ 1.25 mg.

glucose used as a release medium in a control experiment (Fig. 4). Approximately 15% of catalase load released from MNP during this initial burst phase within 15 min in plasma. No further release of the enzyme was observed afterwards, with about 85% of catalase remaining associated with MNP after 48 h of exposure to plasma.

The resistance of MNP-encapsulated catalase to external proteolysis by pronase was determined with two experimental endpoints. First, tracing of residual radiolabeled catalase in the MNP revealed that about 20–30% of the enzyme loaded into MNP was protected from proteolysis in the loading range studied (Fig. 5A). Correspondingly, the capacity of MNP-encapsulated catalase to degrade hydrogen peroxide was found to be in a good agreement with the radioisotope tracing results: ~20% of its initial activity was retained by 24 h of exposure to proteases, as opposed to free enzyme that was completely inactivated within 30 min (Fig. 5B).

3.4. Magnetically guided delivery of MNP-catalase into endothelial cells and their protection from oxidative stress

No appreciable MNP cell uptake was observed under non-magnetic control conditions, whereas MNP briefly exposed (10 min) to a high gradient magnetic field exhibited efficient cell association with subsequent internalization and perinuclear distribution (Fig. 6E and F vs. C and D). Quantitative measurements showed that a significant fraction of MNP applied to cells with magnetic exposure was internalized by the 4 h timepoint ($71 \pm 4\%$ and $46 \pm 2\%$ of MNP added at respective doses of 1 and 5 μg per well; Fig. 6G). This is in contrast to substantially smaller MNP amounts, in the range of 3–8%, determined in cells treated without the presence of magnetic field. Further, fluorescent microscopy revealed dramatically higher endothelial uptake of MNP-encapsulated catalase in cells treated under magnetic conditions, but not in the absence of magnetic exposure (Fig. 6F vs. D), which paralleled the respective patterns of MNP internalization in these cells. Cell viability determined 24 h post treatment was not affected by either blank or catalase-loaded MNP in the studied dose range (Fig. 6H). In an additional experiment addressing the effect of MNP on cell growth kinetics, BAEC treated under magnetic conditions with 5 μg MNP/well exhibited a proliferation rate equal to that of untreated cells, both expanding from 15% to 100% confluence by day 4 with no further changes in cell counts at later time points due to contact inhibition.

Magnetically guided endothelial delivery of MNP-encapsulated catalase efficiently protected endothelial cells from hydrogen peroxide induced cell death. The magnetic guidance of catalase-loaded MNP was essential for providing therapeutically adequate levels of antioxidant protection as evidenced by $62 \pm 12\%$ recovery of viable HUVEC after

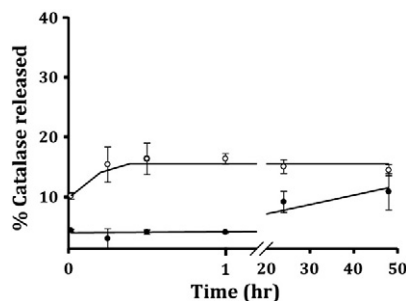


Fig. 4. Release of catalase from MNP. Catalase-loaded MNP were incubated in plasma or aqueous glucose solution (5% w/v) at 37 °C, and the amount of ^{125}I -catalase in the release medium was measured over time by radiotracing after MNP centrifugation. —●— Catalase release in aqueous glucose solution. —○— Catalase release in whole heparinized mouse plasma. Note the biphasic release pattern in plasma with a rapid initial release phase followed by a plateau.

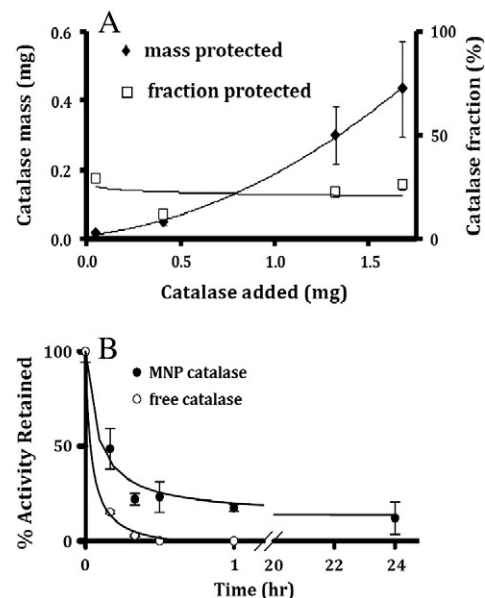


Fig. 5. Protection of catalase mass and activity from proteolysis. A. Mass of MNP-encapsulated catalase protected from proteolysis upon exposure to 0.2 wt.% Pronase at 37 °C for 1 h vs. catalase input. B. Protection of the enzymatic activity of catalase loaded into MNP vs. free catalase upon exposure to 0.2 wt.% Pronase at 37 °C.

exposure to 10 mM hydrogen peroxide for 5 h, whereas only a marginal protective effect was observed with cell treatment under non-magnetic control conditions (Fig. 7A vs. B), as well as with blank MNP added with or without free enzyme (Fig. 7D). No protective effect was exhibited by catalase-loaded non-magnetic nanoparticles (Fig. 7D).

4. Discussion

In the present study a novel type of superparamagnetic nanoparticle formulation (MNP) applicable for targeted delivery of antioxidant enzymes, SOD and catalase, was developed and characterized. The underlying formulation approach is based on the entrapment of biologically active enzymes in non-polymeric MNP formed by controlled aggregation of oleate-stabilized nanocrystalline iron oxide in the presence of calcium, and enables high protein loading yields, controllable MNP size, and magnetic properties adequate for magnetically guided delivery and protection of ROS challenged endothelial cells.

In order to be effective, enzyme-based antioxidant therapy requires strategies for localizing the enzyme with therapeutically adequate functional activity to the site of ROS-mediated injury. Attempts have been made to address this goal by using polymeric nanocarriers. In prior studies with catalase biodegradable polymeric nanoparticles were shown to protect it from proteolysis [21], modulate its release kinetics [22,23], reduce the rate of clearance from circulation by the organs of reticuloendothelial system [24], and enable the inclusion of targeting moieties to direct endothelial specific targeting [15]. The use of organic solvents or high shear emulsification as part of the formulation process and the poor stability of cargo proteins in the particle-forming polymer [7,8] represent challenging aspects of this approach, often associated with a substantial loss of enzymatic activity [23,25].

Calcium oleate-based MNP designed and characterized in this study as antioxidant enzyme carriers have several important advantages, which are highly relevant for the efficient molecular therapy of oxidative stress. Antioxidant enzymes are encapsulated in a non-polymeric matrix of the particles formed under mild conditions.

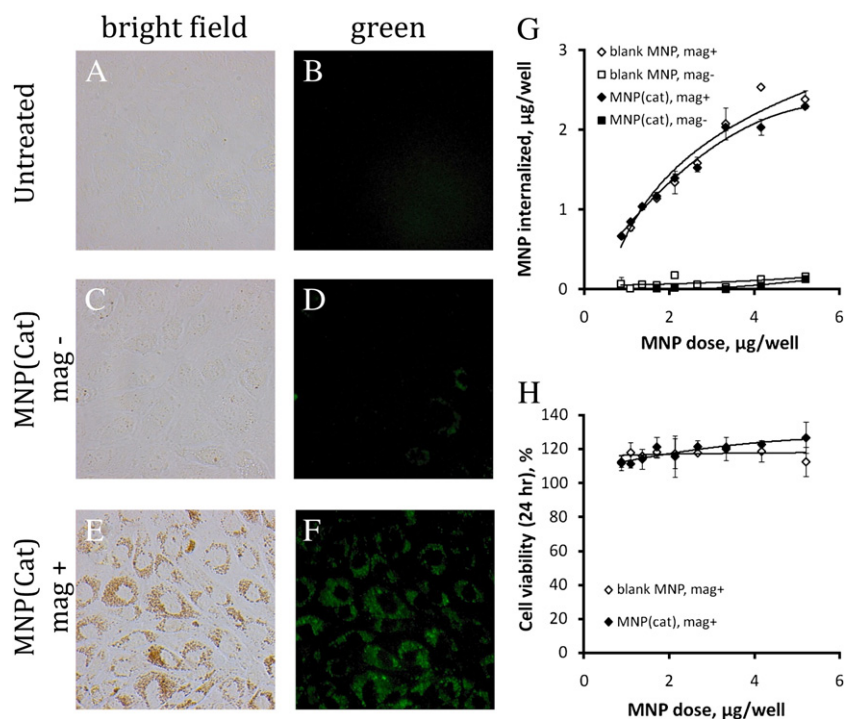


Fig. 6. Magnetic delivery of MNP to cultured bovine aortic endothelial cells. MNP formed with Dylight 488-labeled catalase were applied to cells with or without an exposure to a high gradient magnetic field (10 min), and the cell uptake of MNP and catalase were observed microscopically 4 h post treatment using the bright field and FITC fluorescent channels, respectively, in comparison to untreated cells (A–F). Original magnification $\times 100$. Note the large number of perinuclearly localized MNP in cells treated under magnetic conditions, which is paralleled by a similar cellular distribution pattern of the fluorescent labeled enzyme. Also note the absence of visible MNP or enzyme in non-magnetic control cells. Quantitative assay of cell uptake of blank and catalase-loaded MNP revealed similar patterns with significantly larger amounts of MNP internalized by 4 h after magnetic delivery (G). Cell viability measured 24 h post treatment with MNP under magnetic conditions was not adversely affected (H).

MNP are obtained by aggregation of iron oxide ferrofluid achieved simultaneously with precipitation of calcium oleate in the presence of a non-ionic colloidal stabilizer, Pluronic F-127. Oleate used as a non-

polymeric structural component of MNP in this formulation plays several important roles that are noteworthy:

- 1) It has a distinct affinity for proteins mediated through hydrophobic and electrostatic interactions [26], enabling the high loading efficiency of the cargo enzymes demonstrated in the present study. Importantly, our results indicate that the association of catalase with calcium oleate-based MNP remains stable over a period of at least 48 h upon dilution with plasma. This is in an obvious requirement for efficient protection of catalase, otherwise highly susceptible to proteolysis, from inactivation, and is in agreement with the high levels of enzymatic activity retained by MNP-encapsulated catalase after exposure to pronase observed in this study;
- 2) Oleate anion strongly associates with the iron oxide surface and is essential for the high incorporation yield of small-sized, superparamagnetic nanocrystals in the nanoparticles, thereby providing the latter with a strong magnetic responsiveness in the absence of significant remanence. The resultant superparamagnetic MNP are thus unlikely to irreversibly aggregate upon exposure to a magnetic field, which is necessary for their safe clinical use, yet they can be effectively guided by a magnetic force, which makes them an attractive candidate for targeted delivery applications;
- 3) The capacity of oleate, highly water-soluble as a sodium salt, to spontaneously precipitate as nanoparticles with controllable size upon addition of divalent calcium cations in the presence of a suitable colloidal stabilizer enables formation of the fatty acid-based nanoparticles under strictly aqueous conditions, without utilizing organic solvents typically employed for making polymeric carriers. This mechanism of MNP formation relying on the controlled aggregation/precipitation rather than emulsification appears to be responsible for the improved retention of biological activity by the nanoencapsulated enzymes observed in this study in comparison to previous publications [25];

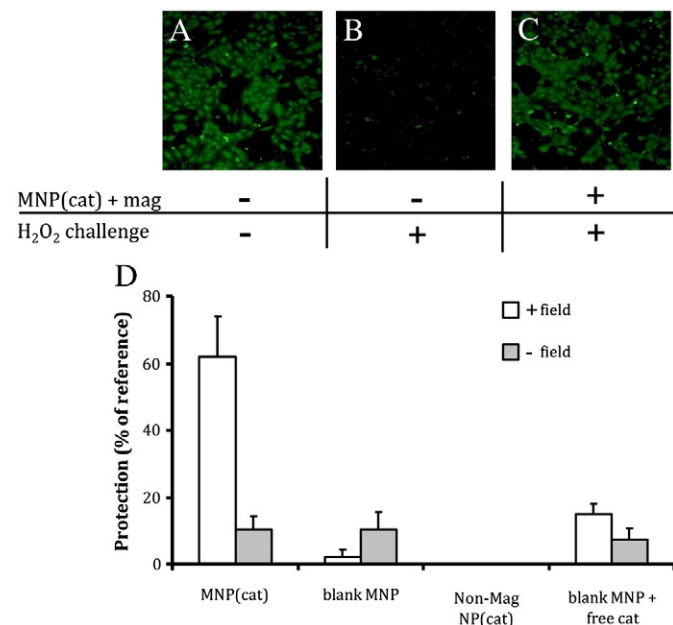


Fig. 7. Protection of HUVEC from oxidative stress through magnetic delivery of catalase loaded MNP. Viability of cells pretreated with MNP and exposed to 10 mM hydrogen peroxide for 5 hour was determined fluorimetrically after staining with Calcein AM. A. Untreated cells used as a reference. B. Cells exposed to hydrogen peroxide only (no protection). C. Cells treated under magnetic conditions with MNP-encapsulated catalase. Original magnification $\times 100$. D. Quantification of the viability of hydrogen peroxide-challenged cells treated with catalase-loaded MNP in the presence of a high gradient magnetic field in comparison to controls.

4) Oleate is an endogenous substance that belongs to the class of monounsaturated fatty acids, and is an essential element in the composition of triglycerides and phospholipids in living cells and tissues. Its metabolism and *in vivo* elimination pathways have been extensively studied, and its biocompatibility, both as a nutrient and as a delivery system component, has been well-established [27,28]. Furthermore, it has also been shown to have a vasculo-protective effect of its own [29], in part mediated by ROS scavenging [30,31]. This property of oleate can potentially explain the small, yet detectable protective effect on cultured endothelial cells exhibited by blank calcium oleate-based MNP used as a control in the present study (Fig. 7D). Interestingly, this is in contrast with the absence of any measurable levels of protection observed with catalase-loaded non-magnetic particles. Since the latter are not influenced by the high gradient field, and are thus not subject to the magnetically mediated uptake enhancement, their interaction with cells within the time frame of the cell protection experiment was likely inefficient, being rate-limited by their slower sedimentation kinetics [32] compared to the iron oxide-loaded MNP possessing a higher density.

As demonstrated by our results, the inclusion of iron oxide, while not essential for the formation of calcium oleate-based nanoparticles, provided the formulations with a capacity for enhanced cellular uptake driven by a high gradient magnetic field. Practically, the sufficiently rapid kinetics of endothelial uptake of catalase-loaded MNP and their cargo enzyme required for achieving the protective effect in ROS-challenged endothelial cells were observed within a clinically relevant exposure time only with magnetic guidance, but not in the absence of a magnetic field and/or with non-magnetic control nanoparticles. This observation confirming the essential dependence of the protective effect mediated by MNP-encapsulated catalase on the endothelial uptake of the carrier emphasizes the importance of implementing a cell-targeted delivery strategy for optimal antioxidant defense.

In the previous studies [33] our group has explored the feasibility of magnetically targeted delivery as an experimental approach aimed at preventing in-stent restenosis, a life-threatening proliferative condition triggered by the trauma caused by stent deployment in atherosclerotic vessels. Our results suggested that the deep-penetrating magnetizing effect of a strong uniform field inducing high gradients on a stainless steel stent and generating a magnetic force acting on MNP, can provide the physical basis for targeted drug, gene or cell delivery to injured arteries [33–35]. In combination with this magnetic guidance strategy, antioxidant enzyme-loaded MNP whose efficacy has been demonstrated in the present study may be an interesting candidate for a stent-targeted antirestenotic therapy. A rationale for exploring the potential of antioxidant enzymes, SOD and catalase, either alone or in combination, for preventing restenosis is based on the major contribution of ROS to the cascade of events eventually resulting in the vessel reobstruction [36,37], with a proof-of-concept provided in previous studies using gene vectors encoding these proteins [38,39].

Several additional aspects pertaining to the utility of calcium oleate-based MNP for cell targeting have remained beyond the scope of the present study. One example is the capacity of MNP decorated with Pluronic F-127 for surface modifications enabling their affinity binding to cell-specific antigens (E. Hood et al., manuscript in preparation). A combination of physical guidance with cell-specific targeting has a potential to significantly extend the range of clinical applications and greatly improve the efficacy and safety of the experimental therapy. The utility of our formulation approach for encapsulation and targeted delivery of biologically active proteins other than SOD and catalase has also remained unexplored. However, based on our findings it is likely that it can be successfully applied with necessary modifications to a broad range of proteins contributing to the design of safer and more efficient clinical therapies.

5. Conclusions

This study describes a novel biocompatible magnetic nanocarrier system suitable for efficient encapsulation of antioxidant enzymes, SOD and catalase, with preserved biological activity. The protection of enzymatic activity from proteolysis by encapsulation in MNP was further demonstrated with catalase, a larger and more labile enzyme, which is therefore more challenging to protect. Furthermore, via magnetic targeting the carrier system demonstrated a therapeutic effect by combating a severe oxidative insult *in vitro*. We conclude that this novel type of magnetically responsive nanoparticles can be used for encapsulation, protection and targeted delivery of antioxidant enzymes, and has a potential to provide a new approach for enzyme-mediated therapy of pathologies related to oxidative stress.

Acknowledgements

The authors would like to thank Vladimir Shuvaev for assistance in determination of SOD activity, Ann-Marie Chacko for fluorescent labeling of catalase, and Eric Simone for particle characterization advice. This work was funded by the National Institute of Health (NIH RO1 HL073940, RO1 HL087036 and PO1 HL079063) (VRM, EH) and the National Center for Research Resources (Grant number UL1RR024134), the Transdisciplinary Program in Translational Medicine and Therapeutics of the Institute for Translational Medicine and Therapeutics (ITMAT), The Cardiac Center at the Children's Hospital of Philadelphia and the American Heart Association (Beginning Grant-in-Aid) (MC). Also support was provided from both the NIH (HL 72108) and the William J. Rashkind Endowment of the Children's Hospital of Philadelphia (RJJL).

References

- [1] S. Laurent, D. Forge, M. Port, A. Roch, C. Robic, L. Vander Elst, R.N. Muller, Magnetic iron oxide nanoparticles: synthesis, stabilization, vectorization, physicochemical characterizations, and biological applications, *Chem. Rev.* 108 (6) (2008) 2064–2110.
- [2] M. Chorny, B. Polyak, I.S. Alferiev, K. Walsh, G. Friedman, R.J. Levy, Magnetically driven plasmid DNA delivery with biodegradable polymeric nanoparticles, *FASEB J.* 21 (10) (2007) 2510–2519.
- [3] M. Namdeo, S. Saxena, R. Tankhiwale, M. Bajpai, Y.M. Mohan, S.K. Bajpai, Magnetic nanoparticles for drug delivery applications, *J. Nanosci. Nanotechnol.* 8 (7) (2008) 3247–3271.
- [4] O. Veisich, J.W. Gunn, F.M. Kievit, C. Sun, C. Fang, J.S. Lee, M. Zhang, Inhibition of tumor-cell invasion with chlorotoxin-bound superparamagnetic nanoparticles, *Small* 5 (2) (2009) 256–264.
- [5] H.L. Ma, X.R. Qi, W.X. Ding, Y. Maitani, T. Nagai, Magnetic targeting after femoral artery administration and biocompatibility assessment of superparamagnetic iron oxide nanoparticles, *J. Biomed. Mater. Res. A* 84 (3) (2008) 598–606.
- [6] M. Lewin, N. Carlesso, C.H. Tung, X.W. Tang, D. Cory, D.T. Scadden, R. Weissleder, Tat peptide-derivatized magnetic nanoparticles allow *in vivo* tracking and recovery of progenitor cells, *Nat. Biotechnol.* 18 (4) (2000) 410–414.
- [7] S.P. Schwendeman, Recent advances in the stabilization of proteins encapsulated in injectable PLGA delivery systems, *Crit. Rev. Ther. Drug Carrier Syst.* 19 (1) (2002) 73–98.
- [8] C.F. van der Walle, G. Sharma, M. Ravi Kumar, Current approaches to stabilising and analysing proteins during microencapsulation in PLGA, *Expert Opin. Drug Deliv.* 6 (2) (2009) 177–186.
- [9] S.S. Pai, R.D. Tilton, T.M. Przybycien, Poly(ethylene glycol)-modified proteins: implications for poly(lactide-co-glycolide)-based microsphere delivery, *AAPS J.* 11 (1) (2009) 88–98.
- [10] E. Rytting, J. Nguyen, X. Wang, T. Kissel, Biodegradable polymeric nanocarriers for pulmonary drug delivery, *Expert Opin. Drug Deliv.* 5 (6) (2008) 629–639.
- [11] M. Soory, Relevance of nutritional antioxidants in metabolic syndrome, ageing and cancer: potential for therapeutic targeting, *Infect. Disord. Drug Targets* 9 (4) (2009) 400–414.
- [12] N.R. Madamanchi, Z.S. Hakim, M.S. Runge, Oxidative stress in atherogenesis and arterial thrombosis: the disconnect between cellular studies and clinical outcomes, *J. Thromb. Haemost.* 3 (2) (2005) 254–267.
- [13] D.G. Harrison, M.C. Gongora, Oxidative stress and hypertension, *Med. Clin. North Am.* 93 (3) (2009) 621–635.
- [14] H. Cai, K.K. Griendling, D.G. Harrison, The vascular NAD(P)H oxidases as therapeutic targets in cardiovascular diseases, *Trends Pharmacol. Sci.* 24 (9) (2003) 471–478.
- [15] T.D. Dziubla, A. Karim, V.R. Muzykantov, Polymer nanocarriers protecting active enzyme cargo against proteolysis, *J. Control. Release* 102 (2) (2005) 427–439.

- [16] V.V. Shuvaev, T. Dziubla, R. Wiewrodt, V.R. Muzykantov, Streptavidin-biotin crosslinking of therapeutic enzymes with carrier antibodies: nanoconjugates for protection against endothelial oxidative stress, *Methods Mol. Biol.* 283 (2004) 3–19.
- [17] T.D. Sweitzer, A.P. Thomas, R. Wiewrodt, M.T. Nakada, F. Branco, V.R. Muzykantov, PECAM-directed immunotargeting of catalase: specific, rapid and transient protection against hydrogen peroxide, *Free Radical Biol. Med.* 34 (8) (2003) 1035–1046.
- [18] J.M. McCord, I. Fridovich, Superoxide dismutase. An enzymic function for erythrocyte hemocuprein (hemocuprein), *J. Biol. Chem.* 244 (22) (1969) 6049–6055.
- [19] V.V. Shuvaev, S. Tliba, M. Nakada, S.M. Albelda, V.R. Muzykantov, Platelet-endothelial cell adhesion molecule-1-directed endothelial targeting of superoxide dismutase alleviates oxidative stress caused by either extracellular or intracellular superoxide, *J. Pharmacol. Exp. Ther.* 323 (2) (2007) 450–457.
- [20] S.J. Stachelek, I. Alferiev, H. Choi, A. Kronsteiner, P. Uttayarat, K.J. Gooch, R.J. Composto, I.W. Chen, R.P. Heibel, R.J. Levy, Cholesterol-derivatized polyurethane: characterization and endothelial cell adhesion, *J. Biomed. Mater. Res. A* 72 (2) (2005) 200–212.
- [21] K.P. Rao, Recent developments of collagen-based materials for medical applications and drug delivery systems, *J. Biomater. Sci., Polym. Ed.* 7 (7) (1995) 623–645.
- [22] T.D. Dziubla, V.V. Shuvaev, N.K. Hong, B.J. Hawkins, M. Madesh, H. Takano, E. Simone, M.T. Nakada, A. Fisher, S.M. Albelda, V.R. Muzykantov, Endothelial targeting of semi-permeable polymer nanocarriers for enzyme therapies, *Biomaterials* 29 (2) (2008) 215–227.
- [23] T.D. Dziubla, V.R. Muzykantov, Synthetic carriers for vascular delivery of protein therapeutics, *Biotechnol. Genet. Eng. Rev.* 22 (2006) 267–298.
- [24] S.M. Moghimi, J. Szebeni, Stealth liposomes and long circulating nanoparticles: critical issues in pharmacokinetics, opsonization and protein-binding properties, *Prog. Lipid Res.* 42 (6) (2003) 463–478.
- [25] U. Bilati, E. Allemann, E. Doelker, Nanoprecipitation versus emulsion-based techniques for the encapsulation of proteins into biodegradable nanoparticles and process-related stability issues, *AAPS PharmSciTech* 6 (4) (2005) E594–604.
- [26] S.Y. Chang, N.Y. Zheng, C.S. Chen, C.D. Chen, Y.Y. Chen, C.R. Wang, Analysis of peptides and proteins affinity-bound to iron oxide nanoparticles by MALDI MS, *J. Am. Soc. Mass. Spectrom.* 18 (5) (2007) 910–918.
- [27] R.G. Strickley, Solubilizing excipients in oral and injectable formulations, *Pharm. Res.* 21 (2) (2004) 201–230.
- [28] C. Wolfrum, F. Spener, Fatty acids as regulators of lipid metabolism, *Eur. J. Lipid Sci. Technol.* 102 (2000) 746–762.
- [29] M. Massaro, R. De Caterina, Vasculoprotective effects of oleic acid: epidemiological background and direct vascular antiatherogenic properties, *Nutr. Metab. Cardiovasc. Dis.* 12 (1) (2002) 42–51.
- [30] R. De Caterina, W. Bernini, M.A. Carluccio, J.K. Liao, P. Libby, Structural requirements for inhibition of cytokine-induced endothelial activation by unsaturated fatty acids, *J. Lipid Res.* 39 (1998) 1062–1070.
- [31] N.A. Porter, S.E. Caldwell, K.A. Mills, Mechanisms of free radical oxidation of unsaturated lipids, *Lipids* 30 (4) (1995) 277–290.
- [32] D. Luo, W.M. Saltzman, Enhancement of transfection by physical concentration of DNA at the cell surface, *Nat. Biotechnol.* 18 (8) (2000) 893–895.
- [33] B. Polyak, I. Fishbein, M. Chorny, I. Alferiev, D. Williams, B. Yellen, G. Friedman, R.J. Levy, High field gradient targeting of magnetic nanoparticle-loaded endothelial cells to the surfaces of steel stents, *Proc. Natl. Acad. Sci. U. S. A.* 105 (2) (2008) 698–703.
- [34] M. Chorny, I. Fishbein, R.J. Levy, Stent-targeted delivery of paclitaxel-loaded biodegradable nanoparticles mediated by a uniform field induced magnetization effect inhibits restenosis in the rat carotid model, *Circulation* 118 (2008) S960–S961.
- [35] B.B. Yellen, M. Chorny, I. Fishbein, D.N. Williams, C.M. Klingerman, I.S. Alferiev, O. Nyanguile, G. Friedman, R.J. Levy, Nanoparticle Mediated Gene Delivery to Magnetized Implants, *Mol. Ther.* 11 (2005) S355–S355.
- [36] P.F. Leite, M. Liberman, F. Sandoli de Brito, F.R. Laurindo, Redox processes underlying the vascular repair reaction, *World J. Surg.* 28 (3) (2004) 331–336.
- [37] P. Misra, P.C. Reddy, D. Shukla, G.C. Caldito, L. Yerra, T.Y. Aw, In-stent stenosis: potential role of increased oxidative stress and glutathione-linked detoxification mechanisms, *Angiology* 59 (4) (2008) 469–474.
- [38] J.H. Brasen, O. Leppanen, M. Inkala, T. Heikura, M. Levin, F. Ahrens, J. Rutanen, H. Pietsch, D. Bergqvist, A.L. Levenon, S. Basu, T. Zeller, G. Kloppel, M.O. Laukkanen, S. Yla-Herttuala, Extracellular superoxide dismutase accelerates endothelial recovery and inhibits in-stent restenosis in stented atherosclerotic Watanabe heritable hyperlipidemic rabbit aorta, *J. Am. Coll. Cardiol.* 50 (23) (2007) 2249–2253.
- [39] E. Durand, A. Al Haj Zen, F. Addad, C. Brasselet, G. Caligiuri, F. Vinchon, P. Lemarchand, M. Desnos, P. Bruneval, A. Lafont, Adenovirus-mediated gene transfer of superoxide dismutase and catalase decreases restenosis after balloon angioplasty, *J. Vasc. Res.* 42 (3) (2005) 255–265.